Dual-action smart coatings with a self-healing superhydrophobic surface and anti-corrosion properties

Qian, Hongchang; Xu, Dake; Du, Cuiwei; Zhang, Dawei; Li, Xiaogang; Huang, Luyao; Deng, Leping; Tu, Yunchao; Mol, Johannes M C; Terryn, Herman A.

DOI
10.1039/c6ta10903a

Publication date
2017

Document Version
Accepted author manuscript

Published in
Journal of Materials Chemistry A

Accepted Author Manuscript of http://dx.doi.org/10.1039/C6TA10903A (RSC)

Dual-action smart coating with a self-healing superhydrophobic surface and anti-corrosion properties

Hongchang Qian[a]‡, Dake Xu[a,b]‡, Cuiwei Du[a], Dawei Zhang[a]*, Xiaogang Li[a], Luyao Huang[a], Leping Deng[a], Yunchao Tu[a], Johannes M.C. Mol[c] and Herman A. Terryn[d]

a. Corrosion and Protection Center, Institute for Advanced Materials and Technology, University of Science and Technology Beijing, Beijing 100083, China
b. Institute of Metal Research, China Academy of Sciences, Shenyang, 110016, China
c. Department of Materials Science and Engineering, Delft University of Technology, Delft, The Netherlands
d. Department of Materials and Chemistry, Research Group Electrochemical and Surface Engineering, Vrije Universiteit Brussel, Brussels, Belgium

‡ These authors equally contribute to this work.

*Corresponding author: Dawei Zhang
Email: dzhang@ustb.edu.cn

Abstract

This work introduces a new self-healing superhydrophobic coating based on dual actions by the corrosion inhibitor benzotriazole (BTA) and an epoxy-based shape memory polymer (SMP). Damage to the surface morphology (e.g., crushed areas and scratches) and the corresponding superhydrophobicity is shown to be rapidly healed through a simple heat treatment at 60 °C for 20 min. Electrochemical impedance spectroscopy (EIS) and scanning electrochemical microscopy (SECM) were used to study the anti-corrosion performance of the scratched and the healed superhydrophobic coatings immersed in a 3.5 wt% NaCl solution. The results revealed that the anti-corrosion performance of the scratched coatings was improved upon the incorporation of BTA. After the heat treatment, the scratched superhydrophobic coatings exhibited excellent recovery of the anti-corrosion performance, which is attributed to the closure of the scratch by the shape memory effect and to the improved inhibition efficiency of BTA. Furthermore, we found that the pre-existing corrosion product inside the coating scratch could hinder the scratch closure by the shape memory effect and reduce the coating adhesion in the scratched region. However, the addition of BTA effectively suppressed the formation of corrosion product and enhanced the self-healing and adhesion performance under this condition. Importantly, we also demonstrated that the coating can be autonomously healed within 1 h in an outdoor environment using sunlight as the heat source.

Keywords:

Self-healing coating; superhydrophobic surface; corrosion inhibitor

1. Introduction

Superhydrophobic surfaces are of increasing interest in many different applications because of their self-cleaning[1,2], anti-fouling[3,4], anti-icing[5,6] and anti-corrosion properties[7,8]. A

superhydrophobic surface with a water contact angle (CA) greater than 150° and a sliding angle (SA) lower than 10° can often be obtained by combining rough surface microstructures with low-surface-energy materials[9]. When these surface microstructures are in contact with water, an air film can be trapped within them to provide an extra barrier for the substrate materials. This feature has made superhydrophobic surfaces particularly attractive as candidate coating materials with enhanced anti-corrosion performance[10-14]. However, the delicate microstructures required for superhydrophobicity are prone to damage from physical impacts and scratches, which often leads to a decrease in hydrophobicity and to the loss of the additional barrier effect.

To overcome this problem, self-healing abilities can be introduced into superhydrophobic coatings to enable the repair of the damaged surface chemistry and/or morphology, which can significantly extend their service lives[15-17]. For example, inorganic/organic micro-/nanocontainers have been used in superhydrophobic coatings for storing low-surface-energy materials[18-21]. Physical damage to the coating surfaces autonomously triggered the release and migration of these low-surface-energy materials from the containers to the coating surface, causing the repair of the surface chemistry. However, this approach has no healing effect on the physical damage to the surface microstructures. Until now, very few studies have reported superhydrophobic coatings with self-healing surface microstructures[22-24]. Lynn *et al.* prepared a water-assisted self-healing superhydrophobic coating using layer-by-layer assembly. Because of the water-induced swelling, the critical porous surface microstructures were fully recovered by immersion in water for only 1 min[22]. The use of shape memory polymers (SMPs) provides another promising solution by which coating's bulk integrity and surface morphology can be restored from temporary deformation in response to environmental stimuli such as heat or light[25-26]. For example, self-healing coatings based on poly(ε-caprolactone) (PCL)-containing polyurethanes (PU) SMPs were reported in several previous works[27-29]. By triggering the shape memory effect above the melting temperature of PCL, coating damages were physically closed, leading to the recovery of the corrosion protection of the aluminum or aluminum alloy substrates. The use of SMPs can also endow superhydrophobic coatings with self-healing properties[30,31]. Chen and Yang developed a superhydrophobic surface based on an SMP pillar array[31]. The deformed or tilted SMP pillars could recover their original shapes upon heating to 80 °C. The surface superhydrophobicity was restored correspondingly. To the best of our knowledge, SMP-based superhydrophobic surfaces have not been used for anti-corrosion purposes.

Besides surface properties, it is also important for anti-corrosion coatings to trigger corrosion inhibition when damage occurs. To this end, a major class of self-healing coatings were developed via the incorporation of corrosion inhibitors such as benzotriazole (BTA)[32-34], 8-hydroxyquinoline (8HQ)[35] and cerium-based inhibitors[36,37]. When damage occurs, the corrosion inhibitors leach out and form barrier films by chemical complexation or physical adsorption on the exposed substrates[38-40]. A few recent studies have incorporated corrosion inhibitors to superhydrophobic coatings[41-43]. For example, Zhang *et al.* recently prepared cerium nitrate or BTA-containing superhydrophobic films on aluminum alloy via the electro-assisted deposition of silica microparticles[41]. Results obtained using the scanning vibrating electrode technique (SVET) revealed that the corrosion activity in the scratched area could be effectively suppressed by the corrosion inhibitors, thereby exerting a self-healing corrosion inhibition effect. In another example, Ding *et al.* prepared a self-healing superhydrophobic coating on magnesium alloys based on

self-assembled silica nanoparticles as pH-responsive nanocontainers containing 2-hydroxy-4-methoxy-acetophenone corrosion inhibitor[42]. In both cases, the anti-corrosion properties of the superhydrophobic coatings were healed by the autonomous releases of the corrosion inhibitors upon damaged, whereas the surface morphology and superhydrophobicity were not recovered.

In this work, we developed a new self-healing superhydrophobic coating whose surface properties and anti-corrosion properties were both repairable based on the dual action from an epoxy SMP and a BTA corrosion inhibitor. Physical damage over the coating's surface morphology and superhydrophobicity can be repaired through the shape memory effect triggered by a short heat treatment or exposure to sunlight. The anti-corrosion performance of the coating upon being damaged was restored by the leached BTA corrosion inhibitor within the coating defect. This self-healing effect was further enhanced by repairs of the physical damage in the coating from the shape memory effect.

2. Experimental section

2.1 Materials

Polydimethylsiloxane (PDMS) prepolymer (Sylgard 184 silicone elastomer kit with curing agent) was purchased from Dow Corning. Bisphenol A diglycidyl ether (BADGE), curing agent (Jeffamine D230 and *n*-decylamine) and BTA were supplied by Sigma–Aldrich. Other solvents and reagents were supplied by Sinopharm. The aforementioned chemicals were all used as received.

2.2 Preparation of the superhydrophobic coatings

To prepare the PDMS template, the PDMS prepolymer and the curing agent were mechanically mixed in a w/w ratio of 10 : 1 at 25 °C for 20 min. The mixture was then poured over a flat lotus leaf fixed in an 8 × 8 cm^2 mold, followed by degassing for 20 min. After curing at 60 °C for 24 h, the PDMS template was peeled from the lotus leaf.

For the preparation of each coating, different amounts (1, 3 and 5 wt%) of BTA were ultrasonically dispersed in a solution of BADGE, Jeffamine D230 and *n*-decylamine with a molar ratio of 8 : 1 : 6, which was determined based on a previous report[44]. The coating solution was then spread over a Q235 carbon steel substrate using a rod applicator, followed by curing at 80 °C for 2 h. A second layer of the same coating solution without any BTA was spread onto the first layer to reduce coating defects. Subsequently, the PDMS template was placed on the coating solution, which then was cured for 3 h at 125 °C. After peeling off the PDMS template, we obtained the superhydrophobic surface with a lotus-like microstructure. As shown in Fig. S1, the thickness of all dry coatings was 50 ± 5 μm. The coatings that contained 1, 3 and 5 wt% of BTA are hereinafter referred to as BTA-1%, BTA-3% and BTA-5%, respectively. For comparison, a BTA-free coating was similarly prepared. Similar procedures were also adopted to prepare a BTA-free superhydrophobic coating which only contained BADGE and Jeffamine D230 at a molar ratio of 2 : 1.

2.3 Thermal properties

Differential scanning calorimetry (DSC) was performed using a TA Instruments Q2000. Coating specimens were sealed in hermetic pans and heated from 0 to 80 °C at a rate of 10 °C min^{-1} under

nitrogen. The glass-transition temperature (T_g) values of the specimens including the BTA-containing coatings, the BTA-free coating and the BTA-free coating with only BADGE and Jaffamine D230 were determined at the inflection of the DSC curves.

2.4 Self-healing tests

Two damage types were induced on the superhydrophobic coating surfaces. A steel bar (⌀5 mm) was pressed against the coating under a load of ~10 MPa to obtain crushed microstructures. A cut-through scratch was also prepared using a fresh razor blade. To induce the shape memory effect, the damaged coatings were i) heated in an oven at 60 °C for 20 min or ii) exposed to sunlight for different duration.

2.5 Surface characterization

The morphology of the damaged and the healed coating surfaces was studied by scanning electron microscopy (SEM, FEI Quanta 250) operated at a 10 kV accelerating voltage. The surface roughness of the coatings was measured by confocal laser scanning microscopy (CLSM, KEYENCE VK-X) over an area of 90 μm × 70 μm. The surface hydrophobicity of the coatings was characterized by a Dataphysics OCA20 goniometer. The static water contact angle (CA) was measured by carefully placing a 5 μL water droplet onto the coating surface. The sliding angle (SA) was measured by tilting the coating surface slowly until a 5 μL water droplet could roll off, and the tilted angle was recorded as the SA. The CAs and SAs reported in this study were the average values of five measurements at different areas on each coating. To determine whether BTA layers adsorbed onto the steel surface, Raman spectroscopic analysis was performed in the wavelength range 200–1800 nm over an area of 2 × 2 μm^2 within the coating scratch, using a laser Raman microscope (LabRAM HR Evolution, HORIBA Jobin Yvon) equipped with a 473 nm He–Cd laser excitation source. Elemental analyses were performed by energy dispersive spectrometer (EDS) mapping on an area of 10 × 5 μm^2 on the exposed steel substrates within the coating scratches.

2.6 Corrosion tests

Electrochemical impedance spectroscopy (EIS, PARSTAT 2273) was performed on the damaged and healed superhydrophobic coatings immersed in a 3.5 wt% NaCl solution for up to 15 days at room temperature. A three-electrode system was used, with the coated panel as the working electrode, a platinum foil as the counter electrode and a saturated calomel electrode (SCE) as the reference electrode. The EIS measurements were performed at the open circuit potential in the frequency range from 10^5 to 10^{-2} Hz with a sinusoidal perturbation of 20 mV. After corrosion tests, the corrosion morphologies of the coatings were investigated using an optical stereomicroscope (KEYENCE VHX-2000).

Localized corrosion activities in the scratched regions on the damaged and healed coatings were studied by scanning electrochemical microscopy (SECM, Ametek M370) measurements with the sample immersed in a 3.5 wt% NaCl solution at room temperature. A four-electrode system was used, with the coated panel as the working electrode, a platinum coil as the counter electrode, an SCE as the reference electrode and a platinum microelectrode as the probe. The tip of the platinum microelectrode (10 μm in diameter) was fixed at a tip-sample distance of 25 μm determined by an approach curve. The measurement was performed by scanning the tip over an area of 300 × 300 μm^2 around the scratched region at a scan rate of 50 $\mu m \cdot s^{-1}$ and with a tip potential of −0.75 V (vs.

SCE).

2.7 Pull-off adhesion tests

The scratched BTA-free and BTA-5% coatings were immersed in 3.5 wt% NaCl solution. After different times, the coatings were retrieved and blow dried with cool air, followed by heating at 60 °C for 20 min to induce the shape memory effect. At different distances (0, 2, 4 and 8 mm) from the scratch, steel dollies (3 mm in diameter) were bonded to the coating surface using epoxy glues. After curing for 12h, the adhesion strengths of the coatings were measured by pulling off the dollies from the coating surface using a PosiTest AT-M tester.

3. Results and discussion

3.1 Healing the surface morphology and hydrophobicity

In this study, the damaged surface morphology of the coatings was healed through the thermally triggered shape memory effect of epoxy polymers, which is an entropically driven process governed by the cooperative actions of the netpoints and switching segments[45,46]. In epoxy SMPs, chemical crosslinks serve as the netpoints to define the permanent shape whereas the T_g of the entangled polymer chains (i.e. switching segments) actuate the shape change. The as-prepared superhydrophobic coating surfaces are in their permanent shapes and the polymers chains adopted conformations with the highest entropy[47,48]. At $T < T_g$, the deformation of polymer chains caused by the physical damages to the coating surfaces are fixed due to the lack of the mobility of the switching segments in the glassy state. Heating above the T_g results in the chain relaxation of the switching segments which transfer from the glassy state to the rubbery elastic state. As a result, the molecular chains restore their entropy and lead to the macroscopic "memory" of the original shape of the coating surface[49-50]. As shown in the DSC measurement (Fig. S2), the T_g of the epoxy containing BADGE and Jeffamine D230 is ~ 80 °C, which is too high for the coating to exhibit self-healing behavior in common service environments. Therefore, the diamine curing agent (Jeffamine D230) was substituted with a monoamine (*n*-decylamine) to reduce the crosslink density of the epoxy SMP in this study[44]. The decreased crosslink density resulted in a lower rubbery modulus of the SMP, causing the T_g to decrease to ~ 40 °C. Therefore, the mobility of the switching segments can be activated at a much lower temperature. The DSC curves for the BTA-free, BTA-1%, BTA-3% and BTA 5% coatings exhibited the same T_g, suggesting that the addition of BTA did not change the shape memory ability.

Fig. 1 shows SEM images of the representative superhydrophobic coatings in the intact, damaged and healed states. As shown Fig. 1a, the original coating surface was uniformly covered with columnar structures with an average diameter of ~8 μm, precisely replicating the lotus leaf surface (Fig. S3). The coating surface achieved a superhydrophobic state with a CA of ~153° and an SA of ~6° because of the air film trapped between the water and the columnar structures. In contrast, the epoxy coating without any surface microstructure exhibited a hydrophilic surface with a CA of ~76° (Fig. S4). Fig. 1b shows the coating surface damaged by crushing against a thin steel bar. The columnar structures were flattened, and their diameters were markedly increased to ~12 μm. Because of the reduction of the air-trapping capacity, the coating surface became much more hydrophilic, with a CA of ~70° and an SA > 90° (Fig. 1b). The second form of damage was induced by scratching the coating with a fresh razor blade. As shown in Fig. 1d, the width of the scratch was ~30 μm and plastic deformation was also evident in the nearby region. The

hydrophobicity of the scratched surface was largely maintained (CA of ~140°) because the damage to the surface morphology was limited to the scratched area. However, the scratch was sufficiently wide for water to penetrate, resulting in a pinned water droplet with an SA > 90°.

Fig. 1c and Fig. 1e show the SEM images of the crushed and scratched coating surfaces, respectively, after being repaired at 60 °C for 20 min. The crushed columnar structures regained their original shapes and dimensions. For the scratched coating surface, the scratch was fully closed after heating, leaving only a very small crevice. The deformed region surrounding the scratch also largely recovered to its original morphology. When heated above the T_g, the fixed switching segments of the SMP were re-activated and regained the entropic elastic behavior, making the deformed columnar structures return to their original shape as defined by the chemical crosslinks (netpoints). It should be noted that the shape memory ability had merely physically narrowed the scratch. The fractured interfaces were not re-bonded as molecular interdiffusion was restricted by the chemical crosslinks. Shape recovery of the coating's surface morphology is critical for the healing of its surface hydrophobicity. After being thermally healed, the closed scratch was too narrow for water penetration and both CA and SA returned to their original values (Fig. 1c and Fig. 1e).

Fig. 2 shows the CLSM images, which provide a 3D presentation of the morphological variations before (Fig. 2a) and after the self-healing tests. In the case of the crushed surface (Fig. 2b), the columnar structures became shallow "waves" and the areal surface roughness (S_a) decreased from 2.5 to 1.4 μm (Fig. 3). The healed surface exhibited complete recovery of the surface microstructures and roughness (Fig. 2c and Fig. 3). In Fig. 3d, the S_a value of the area next to the coating scratch remained almost unchanged despite the slight plastic deformation. After healing, only a very thin line was visible at the scratched region (Fig. 2e).

A water-rolling test was also conducted to further demonstrate the healing effect on surface hydrophobicity. Fig. 4 shows snapshots taken from videos of a 10 μL water droplet rolling on coatings under different conditions. Because of the self-cleaning property, the water droplet can easily roll off from the intact (Fig. 4a) and the healed (Fig. 4d) superhydrophobic surfaces at a tilting angle of ~5°. On the damaged surfaces, the water droplet stopped rolling at the crushed (Fig. 4b) and scratched (Fig. 4c) regions, which caused the loss of superhydrophobicity locally. Full videos corresponding to the images in Fig. 4 are provided in the Supporting Information.

3.2 Healing the anti-corrosion properties

One of the key self-healing mechanisms of anti-corrosion coatings is based on the autonomous actions of corrosion inhibitors at the site of damage. To evaluate the self-healing effect by BTA, we scratched the superhydrophobic coatings that contained different amounts of BTA and then immersed the scratched specimens in a 3.5 wt% NaCl solution for EIS measurements (Fig. 5). In Fig. 5a, the Bode plots of EIS results all exhibit two time constants, indicating that corrosion has occurred at the bottom of the scratch. The low-frequency impedance modulus ($|Z|_{0.01Hz}$) of the Bode plots is often used as a relatively intuitive indicator of the anti-corrosion performance of coatings. The evolution of $|Z|_{0.01Hz}$ values during the 15-day immersion was compared among the coatings with different BTA concentrations (Fig. S5). In general, the coatings containing more BTA exhibited higher $|Z|_{0.01Hz}$ values during the entire immersion test. After 15 days, the $|Z|_{0.01Hz}$ values of BTA-free, BTA-1%, BTA-3% and BTA-5% coatings decreased to 1.8×10^3 Ω·cm^2, 7.1 ×

10^3 Ω·cm^2, 1 × 10^4 Ω·cm^2 and 1.6 × 10^4 Ω·cm^2, respectively. Notably, the deterioration of $|Z|_{0.01Hz}$ values slowed with increasing BTA concentration, which shows that the addition of BTA can effectively improve the anti-corrosion performance of the coatings.

Fig. 5b shows the corrosion morphologies of the scratched coatings after immersion in a 3.5 wt% NaCl solution for 15 days. The amount of corrosion products obviously decreased with increasing BTA content. As illustrated in Fig. 5c, the electrolyte penetrating through the scratch caused the BTA to leach from the coating matrix. The dissolved BTA adsorbed on the exposed steel substrate and inhibited the electrochemical corrosion reactions[51]. The BTA adsorption layers can be evidenced by the Raman spectra measured at the bottom of the scratch (Fig. 6a). All BTA-containing coatings exhibited characteristic BTA peaks at 558 cm^{-1}, 639 cm^{-1}, 789 cm^{-1}, 1046 cm^{-1}, 1153 cm^{-1},1200 cm^{-1}, 1288 cm^{-1}, 1393 cm^{-1}, 1447 cm^{-1} and 1577 cm^{-1} (Table S1), whereas the spectrum of the BTA-free coating shows characteristic corrosion product (lepidocrocite) peaks at 250 cm^{-1}, 378 cm^{-1}, 527 cm^{-1} and 647 cm^{-1} (Fig. 6a)[52]. The peak at 1303 cm^{-1} has previously been confirmed to be related to two-magnon scattering[53,54]. From the BTA-free coating to the BTA-5% coating, the increase in the anti-corrosion performance of the damaged coatings was attributed to the greater coverage of the BTA adsorption layer. To confirm this hypothesis, the distributions of C and N were mapped by Energy Dispersive X-ray spectroscopy (EDS) on the exposed substrate inside the scratch (Fig. 6b). It is clear that C and N atoms were more densely distributed as the BTA content increased.

In addition to corrosion inhibition by BTA, the anti-corrosion ability of the coatings in this study were also healed from the thermally induced shape memory effect of the epoxy coatings. After healing at 60 °C for 20 min, the coatings were immersed in a 3.5 wt% NaCl solution and studied by EIS measurements at different exposure times. At the beginning of the immersion, the Bode plots of all the coatings were characterized by a 45° straight line with the $|Z|_{0.01Hz}$ values (Fig. 7a) reaching beyond 2.5 × 10^{10} Ω·cm^2, indicating full repairs of the coatings' anti-corrosion properties. This result is attributed to the closed scratches after heat treatment, in addition to the restoration of air films within the recovered columnar structures of the superhydrophobic surfaces. In the first 3 days of immersion, the Bode plots of all the specimens exhibited a single time constant (Fig. 7a) and similar decreasing rates of |Z| values. This observation suggests that the coating deterioration to this point was caused by progressive water penetration and that the BTA content did not affect the penetration rate. After 5 days of immersion, corrosion began to occur on the steel substrate, most likely within the scratch, where it was most vulnerable to water penetration. In the case of the BTA-free and BTA-1% coatings, the $|Z|_{0.01Hz}$ decreased to values of 3.2 × 10^4 Ω·cm^2 and 2.0 × 10^5 Ω·cm^2, respectively. By contrast, the coatings that contained a higher loading of BTA (BTA-3% and BTA-5%) demonstrated substantial increases in the $|Z|_{0.01Hz}$ values after 5 days of immersion (Fig. S6), indicating that the corrosion activity on the steel substrates was successfully inhibited. As shown in Fig. S4, the $|Z|_{0.01Hz}$ value of the BTA-5% coating was two orders of magnitude greater than that of the BTA-free coating. Compared with the scratched coatings, the thermally healed coatings exhibited markedly improved anti-corrosion performance, as evident from a comparison of the corrosion morphologies in Fig. 5b and Fig. 7b. No obvious corrosion was observed for the BTA-5% coating after 15 days of immersion.

To further demonstrate the healing actions by the shape memory effect and the corrosion inhibitor, SECM was performed for the *in situ* monitoring of the cathodic reaction (i.e., oxygen reduction)

occurring in the scratched area[55,56]. As shown in Fig. 8, no corrosion activity was detected on the intact BTA-free and BTA-5% coating. In the case of the scratched BTA-free coating (Fig. 8a), corrosion obviously occurred in the damaged area after the specimen had been immersed in a 3.5 wt% NaCl solution for 1 day. The oxygen reduction current density measured by the tip of the platinum microelectrode decreased to nearly 0 A, which suggests that all oxygen in the region has been consumed by cathodic reaction of corrosion activity on the exposed substrates[57, 58]. After 3 days, the current density remained at ~0 A, and the corroded area was widened. In Fig. 8b, the scratched area on the BTA-5% coating showed similarly strong corrosion activity as the BTA-free coating after 1 day of immersion. However, after 3 days, the corrosion activity was suppressed by the coverage of the BTA adsorption layer. As a result, more oxygen was available and the oxygen reduction current density at the platinum microelectrode increased to ~8×10^{-10} A. After thermal repair, the coating exhibited no corrosion activity at the scratched area after 1 day of immersion (Fig. 8c). After 3 days, corrosion activity was visible along the scratch; however, the extent of corrosion was much lower than in the other cases, as indicated by the higher oxygen reduction current density at the platinum microelectrode and by the narrower corroded area.

In the healing of anti-corrosion properties, an advantage of SMP-based coatings over inhibitor-containing coatings is the ability to significantly reduce the damaged area in the coatings because of the crack-closure ability. However, the corrosive medium could still penetrate through the closed crack eventually to corrode the metal substrate since the crack is only closed but not bonded by healing agents. Thus, the barrier properties of the healed coatings could not be recovered to the original level, as we have shown in previous studies. For example, we had prepared an SMP-based self-healing coating using UV-cured acrylated PCL-PU[59]. From EIS measurements in 0.05 mol·L^{-1} NaCl solution, we had shown that the $|Z|_{0.01Hz}$ values of the healed coating could be recovered to > 1×10^{8} Ω·cm^2 but still could not reach the value of the original coating (2×10^{9} Ω·cm^2). In a more recent example, we prepared an epoxy-based SMP coating by cross-linking BADGE and neopentyl glycol diglycidyl ether (NDGE) with Jeffamine D230[49]. After the shape memory effect was triggered, the scratched coating had only partially recovered its barrier properties (against immersion in 3.5 wt% NaCl solution), showing a $|Z|_{0.01Hz}$ value of ~1×10^{6} Ω·cm^2 which was over four orders of magnitude lower than that of the original coating. An additional healing agent made of wax microparticles had to be introduced for the complete sealing of the closed crack on the coating.

The present study offers a unique example of a self-healing superhydrophobic coating with a superior healing performance of the anti-corrosion properties which relies on the dual action from the shape memory effect and the corrosion inhibitor (Fig. 7c). After thermally repaired, the scratched superhydrophobic coatings (with or without BTA) exhibited $|Z|_{0.01Hz}$ values > 2.5×10^{10} Ω·cm^2 at the beginning of the immersion in 3.5 wt% NaCl solution. The fully repaired barrier properties are attributed not only to the crack closure but also more importantly to the restoration of air film trapped in the recovered superhydrophobic surface microstructures. The healed superhydrophobic surface can resist water penetration for a certain time. Once the water penetrates through the air films and reaches into the healed scratch, BTA is leached out for active protection of the steel substrate. With the scratch closed, the exposed area of the substrate is greatly reduced, which is helpful for improving the inhibition efficiency of BTA[25, 60].

3.3 Influence of pre-existing corrosion product on the healing performance

The influence of the pre-existing corrosion product on the healing performance of the coatings was studied in further detail. This property is important for practical applications considering that the damaged coating may be already exposed to corrosive environment before the shape memory-based self-healing process can be triggered. The scratched BTA-free and BTA-5% coatings were immersed in a 3.5 wt% NaCl solution. After being exposed for different times, the samples were dried and heated at 60 °C for 20 min. In Fig. 9a, the scratch on the BTA-free coating could not be thermally healed after 3 days of immersion, which could be attributed to the formation of significant corrosion product that had blocked the narrowing of the scratch from the shape memory effect. The corresponding Bode plot of EIS results showed a severe deterioration of the coating's anti-corrosion properties (Fig. $9c_1$). For the BTA-5% coating, the scratch could still be largely closed after 5 days of corrosion (Fig. $9b_3$). However, the remaining crevice was wide enough for penetration of the corrosive media, which resulted in the decrease in the $|Z|_{0.01Hz}$ by one order of magnitude compared to the original value (Fig. $9c_2$). After 7 days of corrosion, the scratch in the BTA-5% coating was no longer healable (Fig. $9b_4$) and the barrier properties were lost (Fig. $9c_2$). Clearly, the BTA adsorption layers had reduced the corrosion effect and effectively delayed the formation of corrosion product, thereby enhancing the shape memory based self-healing performance under this condition.

The influence of the pre-existing corrosion product on the adhesion strength of the thermally-healed coatings was also evaluated by pull-off tests at locations of various distances to the coating scratch. Because of the corrosion product formed beneath the scratched areas, the adhesion strengths for both BTA-free and BTA-5% coatings decreased in closer proximity of the scratch (Fig. 9d). For the BTA-5% coating, the adhesion near the scratches (0 and 2 mm) decreased with longer immersion time because of the increasing amount of corrosion product, while the adhesion at further distances (4 mm and 8 mm) remained at the original value. The results demonstrated that the addition of BTA could also reduce the degradation rate of the coating's adhesion properties in the scratch area by suppressing the formation of corrosion product.

3.4 Autonomous healing under outdoor exposure

An outdoor exposure test was also conducted to determine whether the coating could autonomously heal itself under sunlight, with no external heating source. Under direct irradiation of sunlight, the temperature of the coating surface exceeded 50 °C after only 20 min, while the air temperature was maintained at 32 °C (Fig. 10b). As shown in Fig. 10a, the scratches on the BTA-5% coating surface had fully closed after 1 h of exposure. The corresponding Bode plot of the EIS data show a 45° straight line, which indicates that the anti-corrosion performance was already fully repaired at this point (Fig. 10c). After 7 days of exposure, the recovered surface morphology and anti-corrosion ability were very well maintained. To our best knowledge, this work represents the first demonstration of SMP-based self-healing materials being autonomously repaired in an outdoor service environment, which could broaden the practical applications of these materials.

5. Conclusions

A dual-action smart coating with a self-healing superhydrophobic surface and anti-corrosion

properties was developed on the basis of an epoxy-based SMP containing BTA corrosion inhibitor. The surface morphology and the corresponding superhydrophobicity could be completely healed from physical crushing and scratches after a simple heat treatment at 60 ℃ for 20 min or by direct outdoor exposure to sunlight within 1 h. To heal the anti-corrosion ability, the first mechanism was demonstrated by the inhibiting effect of leached BTA at the coating scratch. The second healing mechanism was achieved via the thermally induced shape memory effect, which resulted in closure of the coating scratch and restoration of the air film trapped in the surface microstructures. This has also improved the inhibition efficiency of BTA because of the reduced area of the exposed steel substrate. Furthermore, in the presence of pre-existing corrosion product, the BTA-containing coatings demonstrated superior scratch closure ability and adhesion strength to the BTA-free coating. Finally, the coating described in this study presented an improved practicality for use in actual outdoor environments because it was able to heal itself using sunlight as a heat source. With self-healing abilities in both surface superhydrophobicity and anti-corrosion properties, this coating has the potential to satisfy long-term durability requirements for corrosion protection in the presence of common external damage.

Acknowledgments

This work is supported by National Natural Science Foundation of China (No. 51401018), the National Basic Research Program of China (973 Program project, No. 2014CB643300), and the Open Fund of Key Laboratory of Marine Environmental Corrosion and Bio-fouling, Institute of Oceanology, Chinese Academy of Sciences (MCKF201609).

References

1 I. Sas, R. E. Gorga, J. A. Joines and K. A. Thoney, *J. Polym. Sci. Pol. Phys.*, 2012, **50**, 824-845.
2 T. Kamegawa, Y. Shimizu and H. Yamashita, *Adv. Mater.*, 2012, **24**, 3697-3700.
3 J. Chapman and F. Regan, *Adv. Eng. Mater.*, 2012, **14**, B175-B184.
4 C. H. Xue, X. J. Guo, J. Z. Ma and S. T. Jia, *ACS appl. Mater. Inter.*, 2015, **7**, 8251-8259.
5 M. Ruan, W. Li, B. Wang, B. Deng, F. Ma and Z. Yu, *Langmuir*, 2013, **29**, 8482-8491.
6 L. B. Boinovich and A. M. Emelyanenko, *Mendeleev Commun.*, 2013, **23**, 3-10.
7 K. Liu, M. Zhang, J. Zhai, J. Wang and L. Jiang, *Appl. Phys. Lett.*, 2008, **92**, 183103.
8 N. Wang, D. Xiong, Y. Deng, Y. Shi and K. wang, *ACS appl. Mater. Inter.*, 2015, **7**, 6260-6272.
9 D. W. Zhang, L. T. Wang, H. C. Qian, X. G. Li, *J. Coat. Technol. Res.*, 2016, **13**, 11-29.
10 C. H. Xue and J. Z. Ma, *J. Mater. Chem. A*, 2013, **1**, 4146-4161.
11 Y. Cheng, S. Lu, W. Xu, H. Wen and J. Wang, *J. Mater. Chem. A*, 2015, **3**, 16774-16784.
12 N. Wang, D. Xiong, Y. Deng, Y. Shi and K. Wang, *ACS appl. Mater. Inter.*, 2015, **7**, 6260-6272.
13 Q. Liu, D. Chen, and Z. Kang, *ACS appl. Mater. Inter.*, 2015, **7**, 1859-1867.
14 D. W. Zhang, H. C. Qian, L. T. Wang and X. G. Li, *Corros. Sci.*, 2016, **103**, 230-241.
15 Y. Li, S. Chen, M. Wu and J. Sun, *Adv. Mater.*, 2014, **26**, 3344-3348.
16 D. Zhu, X. Lu and Q. Lu, *Langmuir*, 2014, **30**, 4671-4677.
17 L. Ionov and A. Synytska, *Phys. Chem. Chem. Phys.*, 2012, **14**, 10497-10502.
18 K. Chen, S. Zhou and L. Wu, *Chem. Commun.*, 2014, **50**, 11891-11894.

19 C. H. Xue, Z. D. Zhang, J. Zhang and S. T. Jia, *J. Mater. Chem. A*, 2014, **2**, 15001-15007.
20 Y. Liu, X. Pei, Z. Liu, B. Yu, P. Yan and F. Zhou, *J. Mater. Chem. A*, 2015, **3**, 17074-17079.
21 Y. Cong, K. Chen, S. Zhou and L. Wu, *J. Mater. Chem. A*, 2015, **3**, 19093-19099.
22 U. Manna and D. M. Lynn, *Adv. Mater.*, 2013, **25**, 5104-5108.
23 S. Chen, X. Li, Y. Li and J. Sun, *ACS nano*, 2015, **9**, 4070-4076.
24 H. Wang, Y. Xue, J. Ding, L. Feng, S. Wang and T. Lin, *Angew. Chem. Int. Edit.*, 2011, **50**, 11433-11436.
25 X. Luo and P. T. Mather, *ACS Macro Lett.*, 2013, **2**, 152-156.
26 I. A. Rousseau and T. Xie, *J. Mater. Chem.*, 2010, **20**, 3431-3441.
27 Y. González-García, J. M. C. Mol, T. Muselle, I. De. Graeve, G. Van. Assche, G. Scheltjens, B. Van Mele and H. Terryn, *Electrochim. Acta*, 2011, **56**. 9619-9626.
28 J. B. Jorcin, G. Scheltjens, Y. Van Ingelgem, E. Tourwé, G. V. Assche, I. De Graeve, B. Van Mele, H. Terryn and A. Hubin, *Electrochim. Acta*, 2010, **55**, 6195-6203.
29 Y. González-García, J. M. C. Mol, T. Muselle, I. De Graeve, G. Van Assche, G. Scheltjens, B. Van Mele and H. Terryn,. *Electrochem. Commun.*, 2011, **13**, 169-173.
30 T. Lv, Z. Cheng, E. Zhang, H. Kang, Y. Liu and L. Jiang, *Small*, 2016.
31 C. M. Chen and S. Yang, *Adv. Mater.*, 2014, **26**, 1283-1288.
32 E. Abdullayev, V. Abbasov, A. Tursunbayeva, V. Portnov, H. Ibrahimov, G. Mukhtarova and Y. Lvov, *ACS Appl. Mater. Inter.*, 2013, **5**, 4464-4471.
33 M. Serdechnova, S. Kallip, M. G. S. Ferreira and M. L. Zheludkevich, *Electrochem. Commun.*, 2014, **41**, 51-54.
34 T. Chen and J. J. Fu, *Nanotechnology*, 2012, **23**, 235605.
35 K. Zhang, L. Wang and G. Liu, *Corros. Sci.*, 2013, **75**, 38-46.
36 J. Carneiro, J. Tedim, S. C. M. Fernandes, C. S. R. Freire, A. J. D. Silvestre, A. Gandini, M. G. S. Ferreira and M. L. Zheludkevich, *Prog. Org. Coat.*, 2012, **75**, 8-13.
37 J. Mardel, S. J. Garcia, P. A. Corrigan, T. Markley, A. E. Hughes, T. H. Muster, D. Lau, T. G. Harvey, A. M. Glenn, P. A. White, S. G. Hardin, C. Luo, X. Zhou, G. E. Thompson and J. M. C. Mol. *Prog. Org. Coat.*, 2011, **70**, 91-101.
38 H. Wei, Y. Wang, J. Guo, N. Z. Shen, D. W. Jiang, X. Zhang, X. R. Yan, J. H. Zhu, Q. Wang, L. Shao, H. F. Lin, S. Y. Wei and Z. H. Guo, *J. Mater. Chem. A*, 2015, **3**, 469-480.
39 J. Custódio, S. Agostinho and A. Simões, *Electrochim. Acta*, 2010, **55**, 5523-5531.
40 B. Ramezanzadeh and M. Rostami, *Appl. Surf. Sci.*, 2017, **392**, 1004-1016.
41 X. F. Zhang, R. J. Chen, Y. H. Liu and J. M. Hu, *J. Mater. Chem. A*, 2016, **4**, 649-656.
42 C. D. Ding, Y. Liu, M. D. Wang, T. Wang and J. J. Fu, *J. Mater. Chem. A*, 2016, **4**, 8041-8052.
43 Y. Liang, M. D. Wang, C. Wang, J. Feng, J. S. Li, L. J. Wang and J. J. Fu, *Nanoscale Res. Lett.*, 2016, **11**, 231.
44 T. Xie and I. A. Rousseau, *Polymer*, 2009, **50**, 1852-1856.
45 A. Lendlein and S. Kelch, *Angew. Chem. Int. Edit.*, 2002, **41**, 2034-2057.
46 M. Behl and A. Lendlein, *Mater. Today*, 2007, **10**, 20-28.
47 T. Xie, *Polymer*, 2011, **52**, 4985-5000.
48 T. Lv, Z. Cheng, D. Zhang, E. Zhang, Q. Zhao, Y. Liu and L. Jiang, *ACS nano*, 2016, **10**, 9379-9386.
49 L. Wang, L. Deng, D. Zhang, H. C. Qian, C. W. Du, X. G. Li, J. M. C. Mol and H. A. Terryn,

Prog. Org. Coat., 2016, **97**, 261-268.
50 Q. Zhao, H. J. Qi and T. Xie, *Prog. Polym. Sci.*, 2015, **49**, 79-120.
51 J. Y. Chen, X. B. Chen, J. L. Li, B. Tang, N. Birbilis and X. G. Wang, *J. Mater. Chem. A*, 2014, **2**, 5738-5743.
52 M. Hanesch, *Geophys. J. Int.*, 2009, **177**. 941-948.
53 Y. S. Cho and Y. D. Huh, *B. Kor. Chem. Soc.*, 2009, **30**, 1413-1415.
54 M. F. Hassana, M. M. Rahmana, Z. P. Guo, Z. X. Chen and H. K. Liu, *Electrochim. Acta*, 2010, **55**, 5006-5013.
55 Y. González-García, J. M. C. Mol, T. Muselle, I. D. Graeve, G. V. Assche, G. Scheltjens, B. van Mele and H. Terryn, *Electrochem. Commun.*, 2011, **13**, 169-173.
56 A. Simões, D. Battocchi, D. Tallman and G. Bierwagen, *Prog. Org. Coat.*, 2008, **63**, 260-266.
57 W. Wang, L. K. Xu, H. Y. Sun, X. B. Li, S. H. Zhao and W. N. Zhang, *J. Mater. Chem. A*, 2015, **3**, 5599-5607.
58 Y. González-García, S. J. García, A. E. Hughes and J. M. C. Mol, *Electrochem. Commun.*, 2011, **13**, 1094-1097.
59 A. Lutz, O. van den Berg, J. Van Damme, K. Verheyen, E. Bauters, I. D. Graeve, F. E. Du Prez, and H. Terryn, *ACS Appl. Mater. Inter.*, 2014, **7**, 175-183.
60 E. D. Rodriguez, X. Luo and P. T. Mather, *ACS Appl. Mater. Inter.*, 2011, **3**, 152-161.

Figures

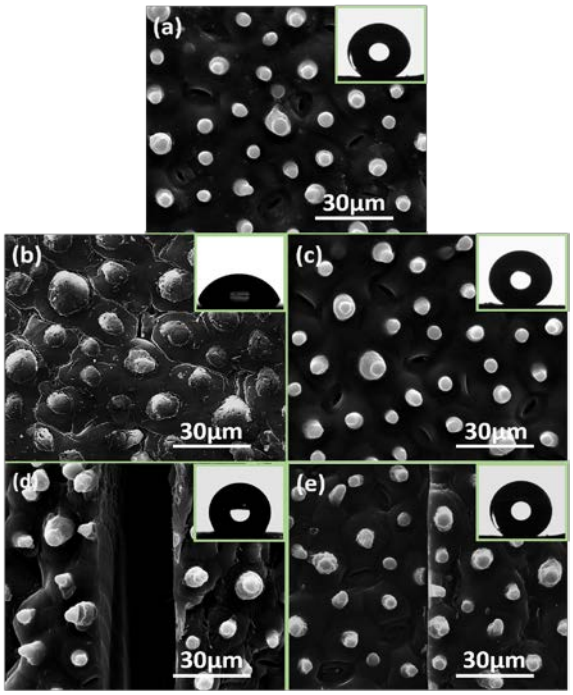

Fig. 1 SEM images of the superhydrophobic coating surfaces: (a) the original surfaces, (b) the crushed surfaces, (d) the scratched surfaces, and (c and e) the healed surfaces. The insets show a water droplet on the coating surfaces.

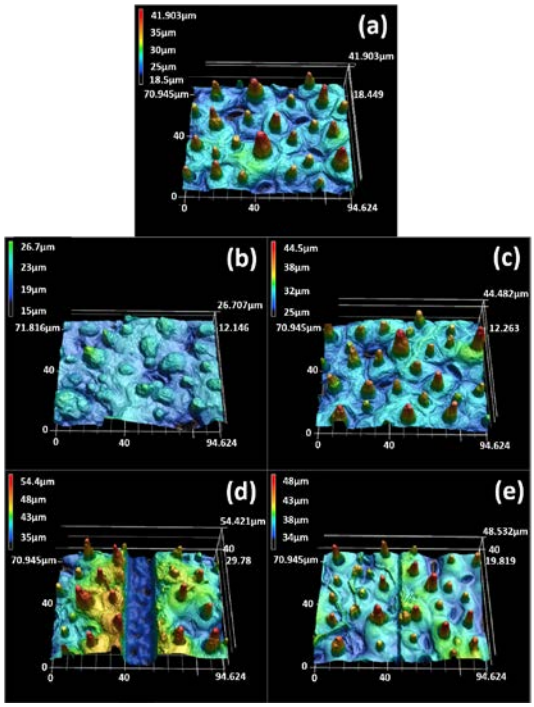

Fig. 2 CLSM images of the superhydrophobic coating surfaces: (a) the original surface, (b) the crushed surface, (c) the crushed surface after healing, (d) the scratched surface, and (e) the scratched surface after healing.

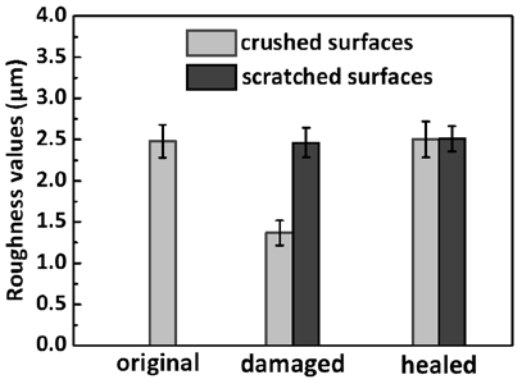

Fig. 3 The evolution of roughness values of damaged superhydrophobic coating surfaces: crushed surfaces (gray) and surfaces beyond the scratched area (black).

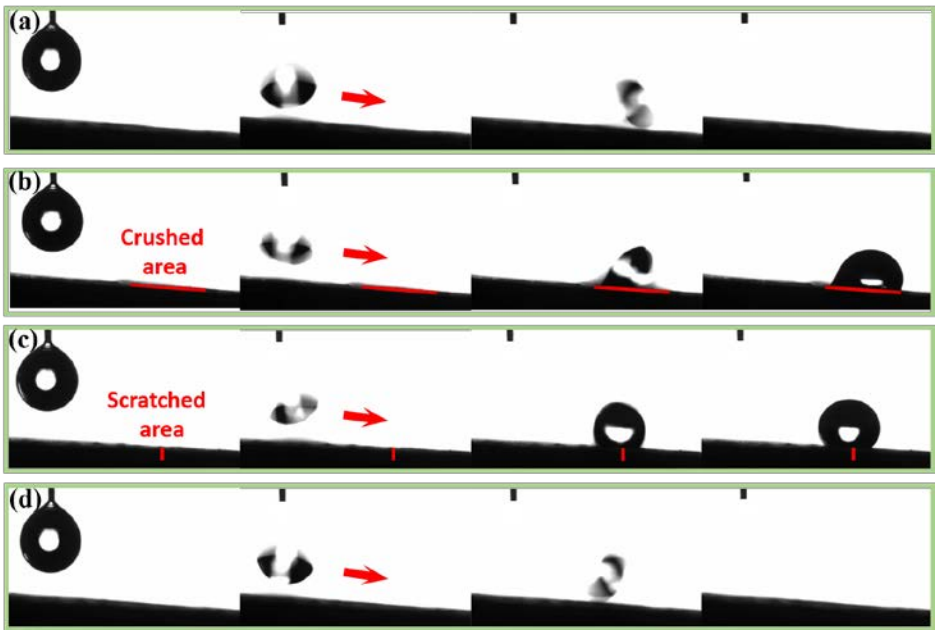

Fig. 4 Video snapshots of the rolling behavior of the water droplet on tilted superhydrophobic coating surfaces: (a) the original surface, (b) the crushed surface, (c) the scratched surface and (d) the healed surface.

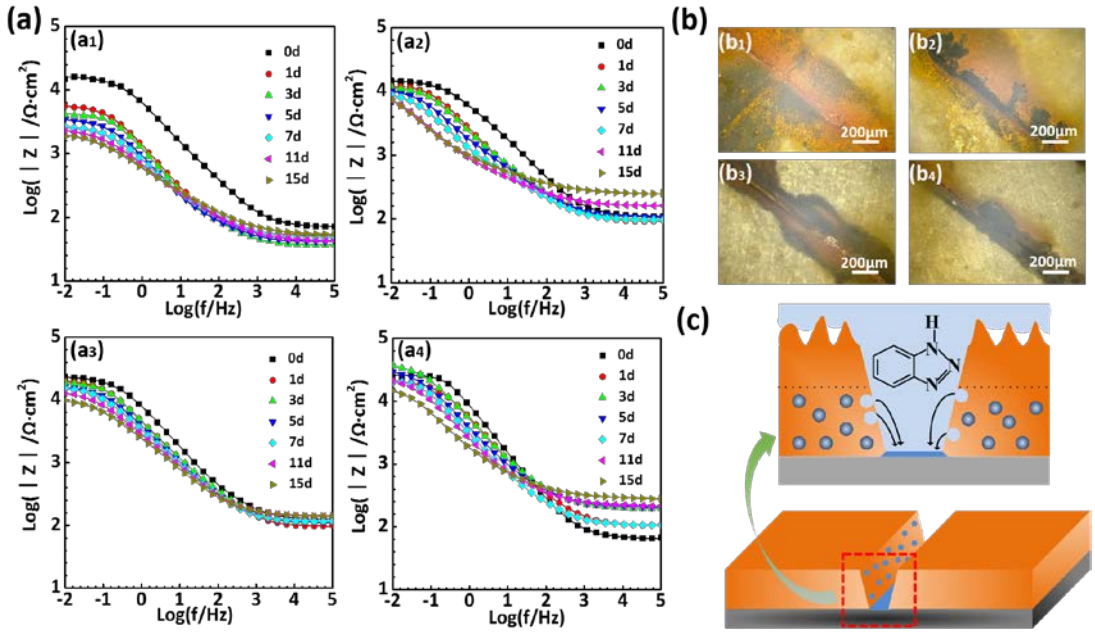

Fig. 5 (a) The evolution of Bode plots of scratched superhydrophobic coatings immersed in a 3.5 wt% NaCl solution for 15 days: (a_1) the BTA-free coating, (a_2) the BTA-1% coating, (a_3) the BTA-3% coating and (a_4) the BTA-5% coating. (b) The optical micrographs of scratched superhydrophobic coatings taken after 15 days of immersion: (b_1) the BTA-free coating, (b_2) the BTA-1% coating, (b_3) the BTA-3% coating and (b_4) the BTA-5% coating. (c) A schematic of the formation of the BTA absorption layer in the scratched area.

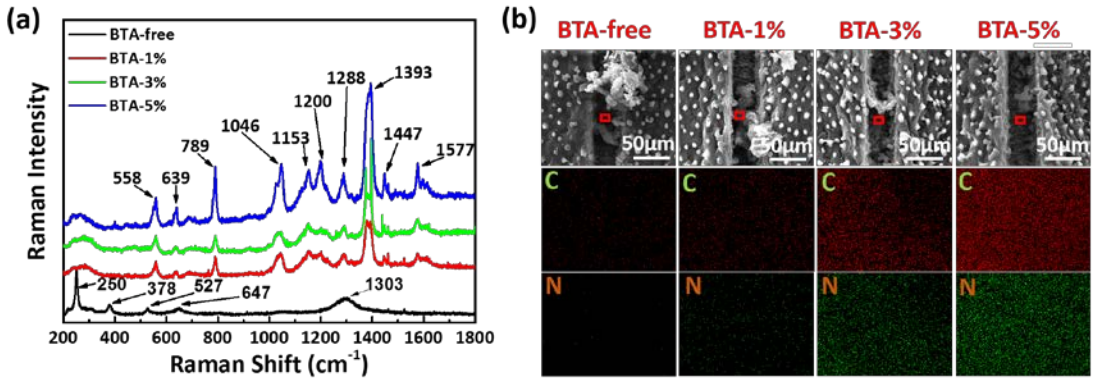

Fig. 6 (a) Raman spectrum and (b) EDS mapping images of the steel surface in the scratched area after 1 day of immersion.

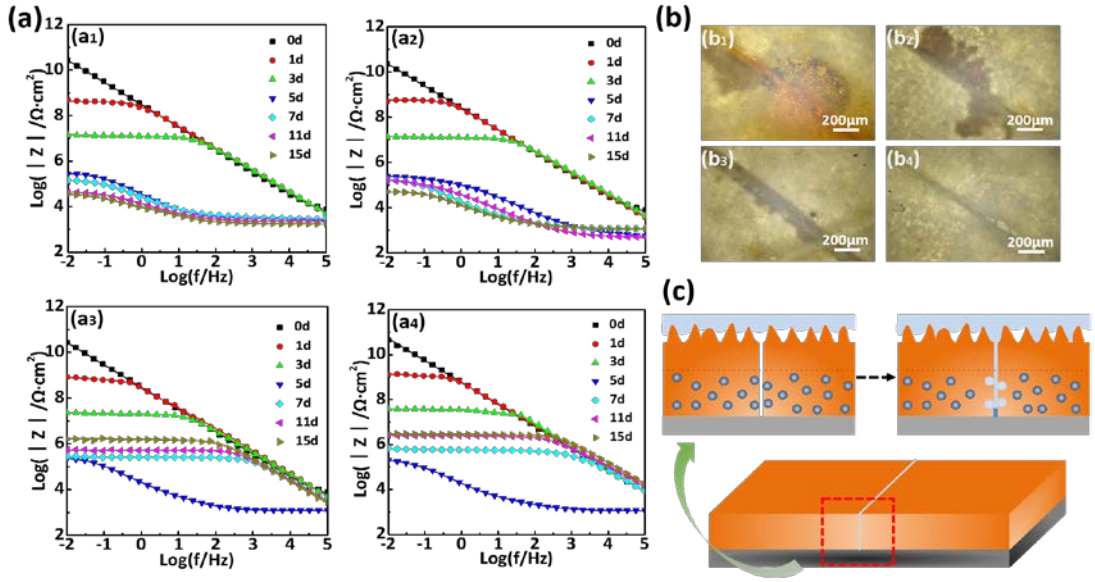

Fig. 7 (a) The evolution of Bode plots of healed superhydrophobic coatings immersed in a 3.5% NaCl solution for 15 days: (a_1) the BTA-free coating, (a_2) the BTA-1% coating, (a_3) the BTA-3% coating and (a_4) the BTA-5% coating. (b) The optical micrographs of healed superhydrophobic coatings taken after 15 days of immersion: (b_1) the BTA-free coating, (b_2) the BTA-1% coating, (b_3) the BTA-3% coating and (b_4) the BTA-5% coating. (c) Schematic of the anticorrosion mechanism of the healed superhydrophobic coatings.

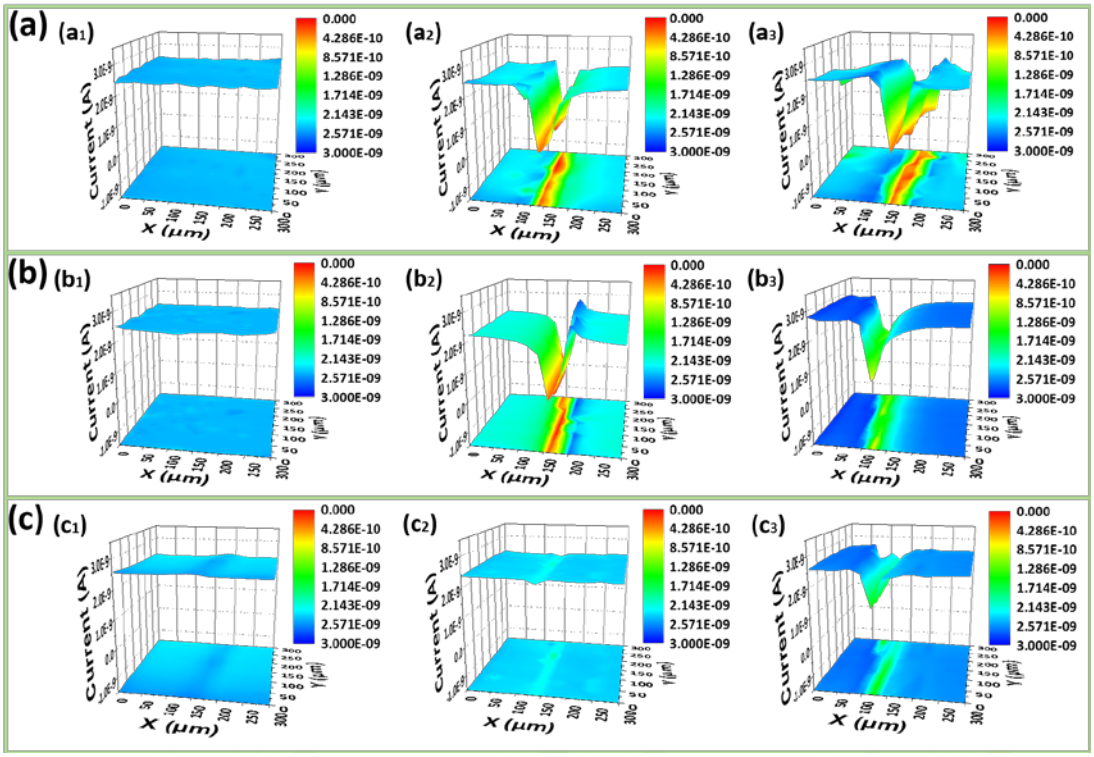

Fig. 8 (a) SECM maps of (a_1) the original BTA-free coating surfaces and the scratched BTA-free coating surfaces immersed in a 3.5 wt% NaCl solution for (a_2) 1 day and (a_3) 3 days. (b) SECM maps of (b_1) the original BTA-5% coating surfaces and the scratched BTA-5% coating surfaces immersed in a 3.5 wt% NaCl solution for (b_2) 1 day and (b_3) 3 days. (c) SECM maps of the healed BTA-5% coating surfaces immersed in a 3.5% NaCl solution for (c_1) 0 days, (c_2) 1 day and (c_2) 3 days.

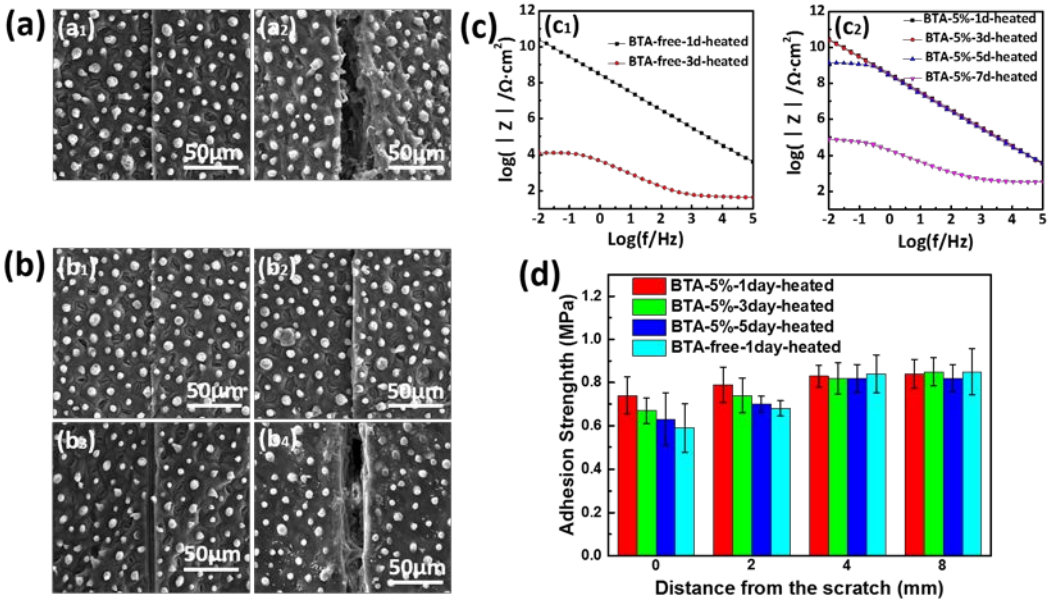

Fig. 9 (a) SEM images of the scratched BTA-free coatings which were immersed in 3.5 wt% NaCl solution for (a_1) 1 day and (a_2) 3 days and subsequently dried and heat treated at 60 °C for 20 min. (b) SEM images of the scratched BTA-5% coatings which were immersed in 3.5 wt% NaCl solution for (b_1) 1 day, (b_2) 3 days, (b_3) 5 days and (b_4) 7 days and subsequently dried and heat treated at 60 °C for 20 min. (c) The corresponding Bode plots of the EIS results for (c_1) the BTA-free coatings and (c_2) the BTA-5% coatings. (d) The pull-off adhesion strengths at different distances to scratches on the heat treated BTA-free and BTA-5% coatings.

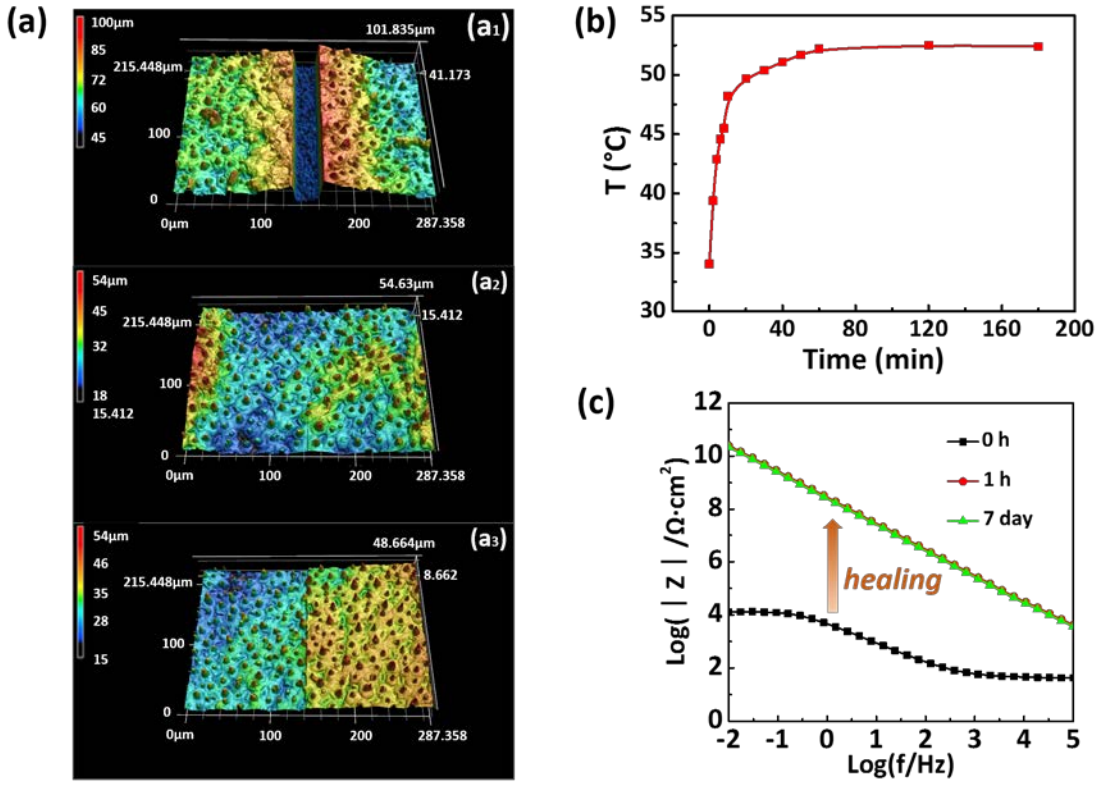

Fig. 10 (a) CLSM images of the scratched BTA-5% coating surfaces after (a_1) 0 h, (a_2) 1 h and (a_3) 1 day of exposure under outdoor environment. (b) The evolution of temperature of the superhydrophobic coating surfaces with time during outdoor exposure. (c) The evolution of Bode plots of the healed BTA-5% coatings after 0 h, 1 h and 7 days of exposure in an outdoor environment.